Journal of the Meteorological Society of Japan, Vol. 78, No. 6, pp. 789–801, 2000

The Gravity Wave Response in the Troposphere around Deep Convection

By Shoichi Shige and Takehiko Satomura

Graduate School of Science, Kyoto University, Kyoto, Japan

(Manuscript received 12 November 1999, in revised form 20 August 2000)

Abstract

The gravity wave response of a quiescent atmosphere to a growing convective cell is investigated, using a non-hydrostatic compressible model. A series of experiments are carried out, categorized as: (i) "MOIST" experiments that employ a parameterization of Kessler warm cloud microphysics, and (ii) "DRY" experiments performed with a prescribed heating function. The heating function used in the DRY experiments is based on the latent heat released and absorbed in the convective cell of the MOIST experiment.

A shallow mode disturbance having a strong updraft at low levels develops near the convective cell when the cell has reached the later growing stage. This disturbance is interpreted as the gravity wave response to higher vertical-mode forcings that increase during the earlier growing stage of the convective cell, and decrease in the later growing stage. For this shallow mode disturbance, not only the increase in the height of heating, but also the narrowness of the width of heating are important. It is found that this shallow mode disturbance is a particular response to a growing convective cell.

The updraft in the low levels of the shallow mode disturbance provides a net vertical displacement. This results from a top-heavy heating profile which forms at the maximum stage of the convective cell. The newly developed cell near the original cell is probably triggered by this net vertical displacement.

1. Introduction

The mechanisms for the maintenance and organization of mesoscale convective systems (MCSs) have been studied extensively. Most of the previous studies have focused on the maintenance of squall lines, or the development of meso-β-scale convective systems into meso-α-scale convective systems.

Modeling studies (Rotunno et al. 1988; Fovell and Ogura 1988, 1989) have addressed the question of determining the environmental conditions that promote squall line development. These studies have focused on interactions between the cold pool and the environmental vertical wind shear. Rotunno et al. (1988) proposed an "optimal state": the updrafts orient vertically if the negative vorticity of the cold pool approximately balances the positive vorticity of the low-level shear.

On the other hand, recent studies on the development of meso-β-scale convective systems into meso-α-scale convective systems, have focused on the role of gravity waves (Nicholls et al. 1991; Mapes 1993; Pandya et al. 1993; McAnelly et al., 1997). These studies have investigated the transient linear response of a quiescent, two-dimensional, non-rotating atmosphere to prescribed heating sources resembling a mature MCS. The vertical heating profiles prescribed by these studies consist of half- and full-wave modes through the troposphere. In the studies, it was assumed that the half-wave-mode heating represented convective heating in the MCS, characterized by condensational heating at all levels, with its maximum heating in the middle troposphere. The full-wave-mode heating was considered to represent stratiform heating in the MCS, characterized by condensational heating in the upper troposphere, and evaporative cooling in the lower troposphere. The resulting MCS heating profile is positive at all levels, but with a maximum value in the upper troposphere. Nicholls et al. (1991) showed that the half-wave-mode disturbance of a downdraft propagates away from the heating, while the full-wave-mode disturbance with an updraft at low levels and a downdraft aloft, trails the half-wave-mode disturbance. Mapes (1993), and McAnelly et al. (1997) suggested that the full-wave-mode disturbance, with an updraft at low levels and a downdraft aloft, provided a net upward displacement at low levels. This upward displacement favored the development of meso-β-scale convective systems into meso-α-scale convective sys-

Corresponding author: Shoichi Shige, Department of Geophysics, Graduate School of Science, Kyoto University, Kyoto 606-8502, Japan. E-mail: shige@kugi.kyoto-u.ac.jp

tems.

Consequently, the importance of the evaporative cooling of rain in the maintenance and organization of MCSs is common to these above mentioned studies, since both the cold pool and the full-wave-mode heating form through the cooling resulting from the evaporation of rain. The evaporative cooling of rain, however, is not always applied to the organization of scattered meso-γ-scale convective systems (convective cells) into meso-β-scale convective systems over the tropical ocean. Parsons et al. (1994) reported that the convectively induced cold pool was shallow over the tropical ocean (about 500 m thick), compared with the thickness of the cold pool over the midlatitude continent (e.g., 1–2 km, Wakimoto 1982). This implies that less rain evaporates over the tropical ocean than over midlatitude continents, because the relative humidity of the lower atmosphere is higher in the tropics than in the midlatitudes. LeMone et al. (1998) reported that convective inhibition (CIN) was small (< 10 J kg^{-1}) over the tropical ocean, enabling convection to develop without an "optimal state" as was described in Rotunno et al. (1988), but with only weak forcing.

The response of the atmosphere to convective cell forcing has received little attention compared with that of the MCS. This is probably because only a few observational studies of the response of the atmosphere to convective cell development have been conducted. The high-frequency, small-scale wave motions excited by a convective cell are very difficult to detect using conventional radiosonde data.

High-frequency waves, however, can be observed by wind profilers having fine time resolutions. For example, Shige (1999) detected mesoscale disturbances in the equatorial western Pacific lower troposphere having periods of 1–2 hours in data from wind profilers with fine time resolution during the Tropical Ocean Global Atmosphere (TOGA) Coupled Ocean–Atmosphere Response Experiment (COARE) (Webster and Lukas 1992). Shige (1999) concluded that the disturbance having a 60-minute period, and a 6-hour duration, was a gravity wave excited by a mesoscale cloud line.

In the present study, focus is placed on the role of gravity waves in the development of a convective cell into a meso-β-scale convective system over the tropical ocean. First, the mechanism of wave excitation by a convective cell is investigated, using a non-hydrostatic compressible model. Next, the role of these gravity waves in the formation of new cells is discussed.

2. The model and experiments

2.1 Numerical model

Use was made of the compressible, non-hydrostatic cloud model, termed the Advanced Regional Prediction System (ARPS) Version 4.0 (Xue et al. 1995), which was developed at the Center for Analysis and Prediction of Storms (CAPS) at the University of Oklahoma. The computations were carried out under a two-dimensional model configuration. The basic environmental state was assumed constant in time and horizontally homogeneous. The Coriolis terms were neglected. The lower and upper boundaries were flat, rigid, and under free slip conditions. A radiation condition (Durran and Klemp 1982) was used at the lateral boundaries. The ARPS model employs a mode-splitting time integration scheme (Klemp and Wilhelmson 1978) that integrates acoustically active and inactive terms separately in two steps. These time steps were chosen as 0.5 and 3 s for the active and inactive terms, respectively, in the present study. A 1.5-order turbulent kinetic energy closure scheme was also used. The surface momentum and heat fluxes, and the solar radiation, were not calculated in the present study. Details of the model have been presented in Xue et al. (1995).

Experiments were performed in order to investigate the gravity waves forced by the latent heat released and absorbed by a growing convective cell. These experiments were classified into two categories: (i) "MOIST" experiments that employed a parameterization of Kessler warm cloud microphysics, and (ii) "DRY" experiments performed with a prescribed heating function instead of the microphysical parameterization. The warm rain microphysics of Kessler in the MOIST experiments considers three categories of water (Klemp and Wilhelmson 1978): water vapor, cloud water, and rain water. The heating function prescribed in the DRY experiments was based on the latent heat released and absorbed by the convective cell in the MOIST experiment. A similar approach has been applied to the mesoscale circulation around squall lines by Pandya and Durran (1996), and Pandya et al. (2000), and stratospheric gravity waves above squall lines by Pandya and Alexander (1999).

The vertical resolution in the MOIST experiments was expanded from 50 m at the lower boundary to approximately 500 m at the top of the domain. This varying vertical resolution was chosen to simulate a shallow cold pool near the lower boundary. The vertical resolution in the DRY experiments was 500 m. In all of the experiments, the horizontal resolution was 500 m. The model domain was 90.0 km in the x direction (horizontal), and 18.5 km in the z direction (vertical). A Rayleigh damping layer having a depth of 6.0 km was included at the top of the domain to reduce the reflection of gravity waves from the upper boundary.

2.2 Experimental design

The major experiments and their parameters are (c.f., Table 1):

Table 1. List of the major experiments. Q_0 and a are the magnitude of the heating function $Q(x,z,t)$, and the half-width, respectively.

Case	category	cloud physical process	Q_0	a
FULL	MOIST	full set		
NOEVAP	MOIST	no evaporation		
SIMPLE	DRY	no	1.0 J kg^{-1} s^{-1}	0.5 km
STRONG	DRY	no	40.0 J kg^{-1} s^{-1}	0.5 km
WIDE	DRY	no	1.0 J kg^{-1} s^{-1}	10.0 km

(1) Case FULL (MOIST). This is the realistic reference experiment in which all of the Kessler warm cloud microphysics are included. In this experiment, heating profiles from the convective cell were obtained and used as the basis for the heating function in the DRY experiments.

(2) Case NOEVAP (MOIST). This is the same experiment as in Case FULL except for the exclusion of the evaporation process of rain in the model. In this experiment, there was no formation of the cold pool. By comparing this case with Case FULL, the importance of the cold pool in the formation of a new cell can be assessed.

(3) Case SIMPLE (DRY). In this experiment, the heating function $Q(x,z,t)$ was prescribed that approximates the temporal and spatial characteristics of the convective cell rather than including the cloud microphysical processes. The heating function $Q(x,z,t)$ is based on the latent heat released and absorbed by the convective cell obtained in Case FULL. To apply a linear analysis to the gravity waves in the results, the magnitude of $Q(x,z,t)$, however, has been reduced to about 40 times smaller than the heating in the convective cell of Case FULL. Details of the prescribed heating function $Q(x,z,t)$ will be discussed in a later section.

(4) Case STRONG (DRY). This experiment is the same as Case SIMPLE, except that the magnitude of $Q(x,z,t)$ is 40 times larger than that of Case SIMPLE, being nearly the same as that of the heating in the Case FULL convective cell. The features in Case STRONG are compared to those in Case SIMPLE to assess the linearity of the gravity wave response to the heating function $Q(x,z,t)$.

(5) Case WIDE (DRY). This is an experiment where $Q(x,z,t)$ has a half-width that is 20 times as wide as that in Case SIMPLE. The magnitude of $Q(x,z,t)$ in this experiment is the same as that in Case SIMPLE. In this experiment, the effects of the horizontal width of $Q(x,z,t)$ on the response are investigated.

The MOIST experiments are initialized with the COARE sounding at Keifu-maru, at 1200 UTC on 6 November, 1992 (Fig. 1), when convection in the area was active. The 1200 UTC sounding was not sufficiently moist to support the height of the convection observed in the GMS data. The relative humidity at heights lower than 2750 m was therefore increased, as shown by the thick solid line in Fig. 1. It should be noted that the numerically simulated features did not vary qualitatively by increasing the low level relative humidity.

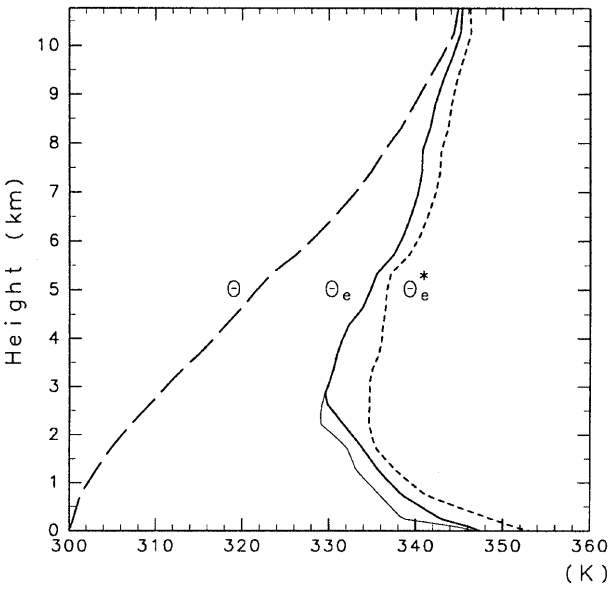

Fig. 1. The smoothed sounding used as input in the MOIST experiments, showing the vertical profiles of potential temperature θ (dashed line), equivalent potential temperature θ_e (solid line), and saturated equivalent potential temperature θ_e^* (dotted line). The profiles are based on the sounding at Keifu-maru, at 1200 UTC on 6 November, 1992. The thin solid line indicates observed equivalent potential temperature.

Convection was initiated by placing an ellipsoidal warm thermal (a maximum potential temperature excess of 2.0 K) having a horizontal radius of 10.0 km, and a vertical radius of 1.5 km. The center of the thermal is located at x = 0.0 km and z = 1.5 km. On the other hand, for the DRY experiments, the gravity wave response of a quiescent atmosphere with constant Brunt-Väisälä frequency N ($= 0.01\ s^{-1}$) to the heating function $Q(x,z,t)$ is investigated.

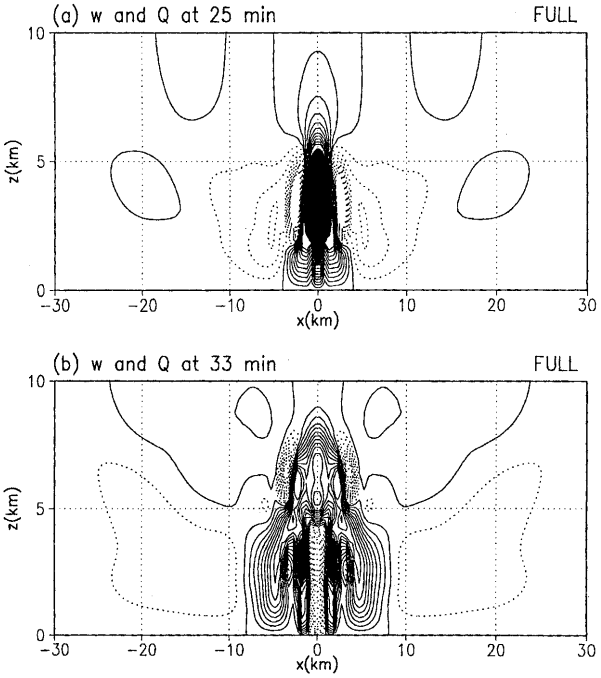

Fig. 2. Time sequence of zonal-height cross section of vertical velocity and latent heat for Case FULL, at (a) 25 min, and (b) 33 min. The contour interval is 0.4 m s^{-1}. Negative contours are dashed lines; zero and positive contours are solid lines. The regions in which the latent heat exceeds 20.0 J kg^{-1} s^{-1} are shaded.

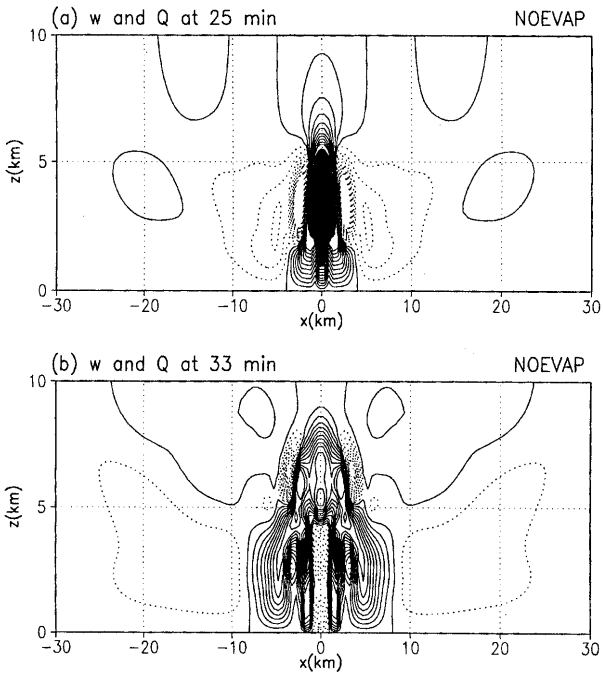

Fig. 3. As in Fig. 2, except for Case NOEVAP.

3. Experimental results

The vertical velocity and latent heat for Case FULL are shown in Fig. 2. A convective cell, initiated by the thermal bubble, is growing at $x = 0.0$ km at $t = 25$ min (Fig. 2a). It is clear from Fig. 2a that a strong low-level updraft occurs near the original cell, from $x = -1.0$ to -3.0 and 1.0 to 3.0 km, whereas a downdraft has formed in the outer regions. By $t =$ 33 min (Fig. 2b), a new cell has formed at $x \approx \pm$ 2.0 km, where the low-level updraft was observed at 25 min. The low-level updraft appears to play an important role in the formation of the new cell. The life time of the original cell initiated by the thermal bubble is about 60 min.

Even in Case NOEVAP, where the evaporation of rain is excluded, the vertical velocity pattern at $t =$ 25 min (Fig. 3a) is nearly the same as that in Case FULL (Fig. 2a). Except for the vertical velocity at $(x, z) =$ (0.0 km, 2.0 km), the vertical velocity pattern at 33 min in Case NOEVAP (Fig. 3b) is also very similar to that in Case FULL (Fig. 2b). These results suggest that the strong low-level updrafts seen in Figs. 2a and 3a are not produced by the cold pool, since the cold pool does not form in Case NOEVAP.

The width of the convective cell heating varies in time and height. At $t = 25$ min (Fig. 2a), the horizontal width for Case FULL at $z = 3.0$ km is about 4.0 km ($x = -2.0$ to 2.0 km), while that at $z = 1.5$ km is about 2.0 km ($x = -1.0$ to 1.0 km). Focus is now placed on the strong low-level updraft seen near the original cell at $t = 25$ min (Fig. 2a), which is expected to play an important role in the formation of the new cell. Therefore, the horizontal width at low levels at 25 min (2.0 km) is considered the horizontal width of the heating in the convective cell. The influence of the horizontal width on the strong low-level updraft is very important. The strong low-level updraft, however, does not vary qualitatively, even when the horizontal width is 4.0 km. These points will be discussed in a later section.

The time sequence of latent heating profiles of the original cell from $t = 5$ min until 30 min for Case FULL is shown in Fig. 4a. These heating profiles are spatially averaged from $x = -1.0$ km to 1.0 km. There are two characteristics of the growing convective cell: 1) the height of the heating increases with time, and 2) the amplitude of the heating increases with time. The original cell reaches its maximum after 30 min. The maximum height of the heating in the convective cell occurs at about 8.8 km. In order to roughly approximate these two characteristics, the heating function used in the DRY experiments is given as:

$$Q(x,z,t)=\begin{cases} Q_0 \dfrac{a^2}{x^2+a^2} \dfrac{1-\cos(2\pi t/T)}{2} \sin\left(\dfrac{\pi z}{H_m(t)}\right), \\ \qquad\qquad (\text{for } 0 \le z \le H_m(t)) \\ 0, \\ \qquad\qquad (\text{for } z > H_m(t)), \end{cases} \tag{1}$$

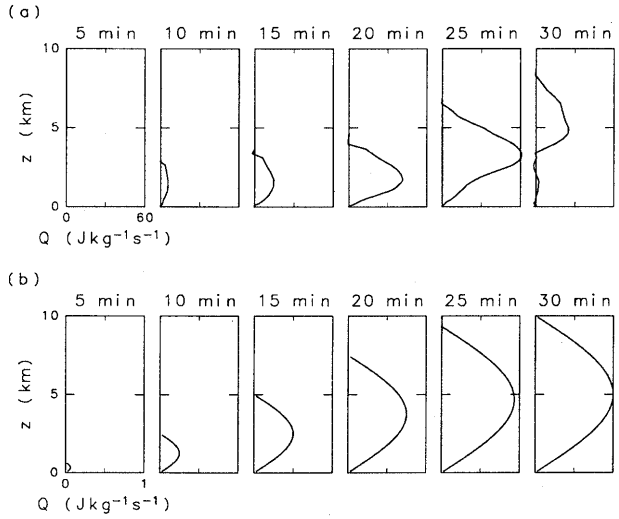

Fig. 4. Time sequences of (a) the heating profiles averaged from $x = -1.0$ km to $x = 1.0$ in Case FULL, and (b) the heating function $Q(x, z, t)$ at $x = 0.0$ km.

where Q_0 is the magnitude of the thermal forcing, a the half-width, and $H_m(t)$ the height of the heating given by

$$H_m(t) = \begin{cases} H\dfrac{1-\cos(2\pi t/T)}{2}, & (\text{for } 0 \le t \le T/2) \\ H, & (\text{for } T/2 < t \le T). \end{cases} \quad (2)$$

Here H equals 10.0 km and $T = 60$ min. The height and amplitude of $Q(x, z, t)$ increase until 30 min, as shown in Fig. 4b. The horizontal structure of $Q(x, z, t)$ is a practical approximation which simplifies the mathematics. The horizontal structure of $Q(x, z, t)$ does not strictly approximate that of the heating in the convective cell, because $Q(x, z, t)$ has a non-zero value, even far from $x = \pm$ 1.0 km. The features of the gravity wave response around the convective cell, however, can be captured qualitatively.

Figures 5a and b show the vertical velocity at t = 25 and 30 min, respectively, for Case SIMPLE where Q_0 = 1.0 J kg^{-1} s^{-1}, and a = 0.5 km (see Table 1). The half-width a = 0.5 km corresponds to a horizontal width of 2.0 km. At t = 25 min (Fig. 5a), a strong updraft is centered at $x = 0.0$ km in the heated region and downdrafts have developed at $x \approx \pm$ 10.0 km. The downdrafts extend throughout the troposphere. It is also clear from Fig. 5a that at $x \approx \pm$ 2.0 km, low-level updrafts have decoupled from the heated region. These features at 25 min found in Case SIMPLE are similar to those at 25 min for Case FULL (Fig. 2a). When $Q(x, z, t)$ reaches its maximum at 30 min, deep-mode downdraft disturbances have moved beyond $x \approx \pm$ 10.0 km (Fig. 5b). Shallow-mode disturbances of an updraft at low levels and a downdraft aloft are seen at $x \approx \pm$ 5.0 km.

Figure 6 shows the response for Case STRONG

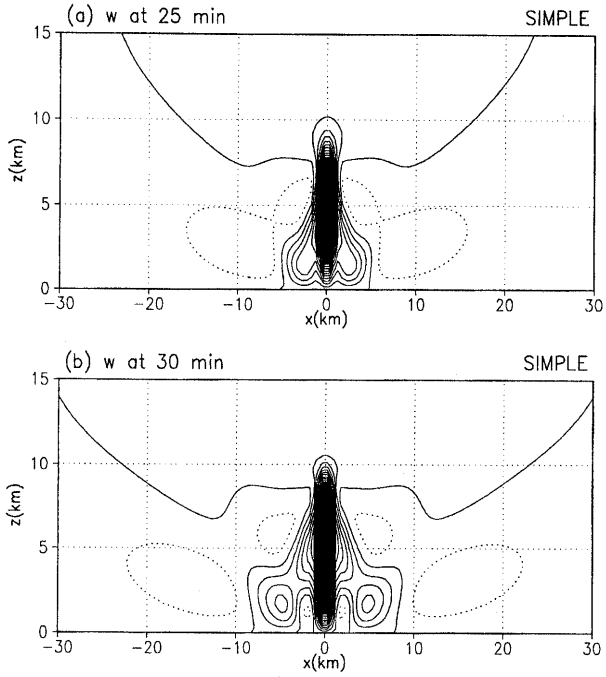

Fig. 5. As in Fig. 2, except for vertical velocity in Case SIMPLE at (a) 25 min and (b) 30 min. The contour interval is 0.01 m s^{-1}. The regions in which the vertical velocity exceeds 0.1 m s^{-1} are shaded.

with Q_0 = 40.0 J kg^{-1} s^{-1}, which is nearly the same as the convective cell heating in Case FULL. Responses in Case STRONG are nearly the same as those in Case SIMPLE with Q_0 = 1.0 J kg^{-1} s^{-1}, as shown in Fig.5: 1) downdrafts have developed at $x \approx \pm$ 10.0 km with low-level updrafts decoupled from the center region of a strong updraft at 25 min (Fig. 5a and Fig. 6a), and 2) deep-mode downdraft disturbances at $x \approx \pm$ 15.0 km with shallow mode disturbances of an updraft at low levels and a downdraft aloft at $x \approx \pm$ 5.0 km are observed at 30 min (Fig. 5b and Fig. 6b). On the other hand, the vertical velocity in Case STRONG is about 40 times greater than that in Case SIMPLE. These results imply a linear relation between Q_0 and the vertical velocity, allowing the application of linear analysis to interpret the results in Case SIMPLE. It may be noted that the vertical wavelength of the shallow-mode disturbance in Case STRONG (Fig. 6b) is somewhat longer than that in Case SIMPLE. This probably results from the updraft at $x = 0.0$ km in Case STRONG being elevated higher than that in Case SIMPLE, owing to nonlinear effects.

When the half-width of the heating function is increased to 10.0 km (Case WIDE, Fig. 7), the results change drastically. A strong updraft is centered at $x = 0.0$ km, and downdrafts have developed on both sides of the strong updraft (Fig. 7a), as well as in Case SIMPLE. The shallow-mode disturbance of an updraft at low levels and a downdraft aloft, however,

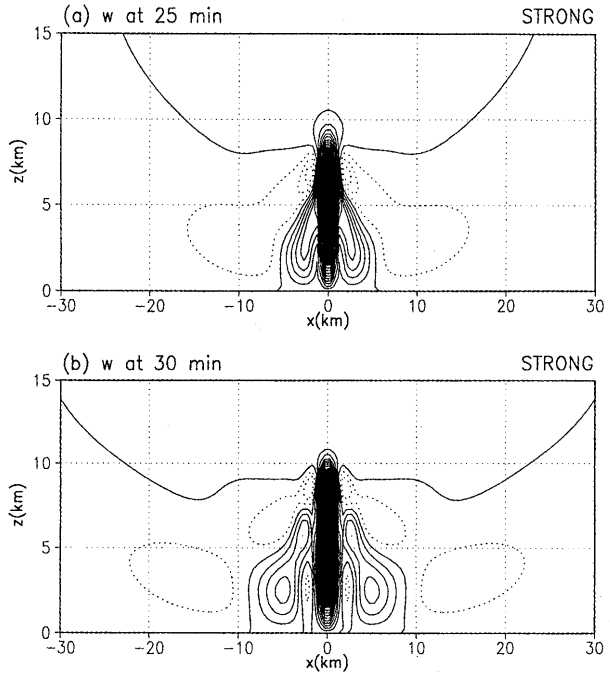

Fig. 6. As in Fig. 2, except for vertical velocity in Case STRONG at (a) 25 min and (b) 30 min. The contour interval is 0.4 m s^{-1}. The regions in which the vertical velocity exceeds 4.0 m s^{-1} are shaded.

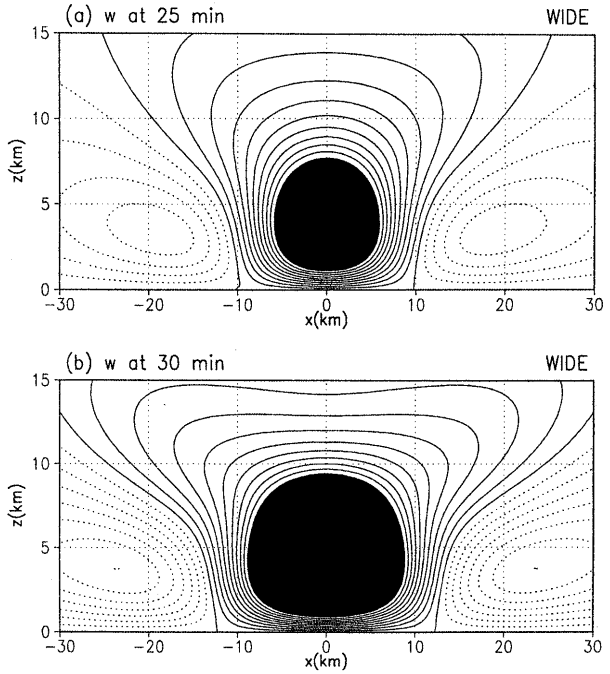

Fig. 7. As in Fig. 2, except for vertical velocity in Case WIDE at (a) 25 min and (b) 30 min. The contour interval is 0.01 m s^{-1}. The regions in which the vertical velocity exceeds 0.1 m s^{-1} are shaded.

can not be found at either $t = 25$ min or 30 min (Fig. 7a and b).

4. Discussion

4.1 Low-level updraft

Discussion is now centered on why the shallow-mode disturbance of an updraft at low levels and a downdraft aloft decouples from the heated region in Case SIMPLE (Fig. 5). This disturbance is very similar to the "n = 2 mode" disturbance of an updraft at low levels and a downdraft aloft as obtained in Fig. 5b of Nicholls et al. (1991). This n = 2 mode disturbance is the gravity wave response to the n = 2 mode heating. The n = 2 mode heating approximates the stratiform heating in the MCS, characterized by condensation in the upper troposphere and evaporation in the lower troposphere. In spite of the similarity in the disturbances, the heating profiles from all cases of the present study do not include stratiform heating. Therefore, the mechanism for the excitation of this shallow-mode disturbance can not be explained by that of the n = 2 mode disturbance discussed by Nicholls et al. (1991).

The x-independent part of the heating function $Q(x, z, t)$ ($0 < z < H_m(t)$: Eq. (1)) is given as

$$\hat{Q}(z,t) = Q_0 \frac{1-\cos(2\pi t/T)}{2} \sin\left(\frac{\pi z}{H_m(t)}\right). \quad (3)$$

Decomposition of $\hat{Q}(z,t)$ (Fig. 4b) into discrete vertical modes $\sin(n\pi z/H_0)$ (Fig. 8a) results in

$$\hat{Q}(z,t) = \sum_{n=1} \hat{Q}_n(t) \sin\left(\frac{n\pi z}{H_0}\right), \quad (4)$$

where H_0 is the maximum height of the decomposed heating, with $H_0 = H = 10.0$ km.

Linear responses to the modes described in Eq. (4) implies that the responses satisfy rigid boundary conditions at $z = 0.0$ km and $z = 10.0$ km.

To examine the effect of a rigid lid at $z = 10.0$ km and the validity of the discussion of using Eq. (4), an experiment that is the same as Case SIMPLE, except for a flat, rigid, and free-slip upper boundary at $z = 10.0$ km (Case RIGID) is conducted. In Case RIGID, a Rayleigh damping layer is not included. Figure 9 shows the response for Case RIGID. Responses found for Case RIGID are nearly the same as those from Case SIMPLE (Fig. 5). That is, 1) downdrafts have developed at $x \approx \pm$ 10.0 km, and low-level updrafts have decoupled from the center region of the strong updraft by 25 min (Fig. 9a), and 2) deep-mode downdraft disturbances develop at $x \approx \pm$ 15.0 km, and at $x \approx \pm$ 5.0 km shallow mode disturbances of an updraft at low levels and a downdraft aloft are observed at 30 min (Fig. 9b). The updraft at low levels and downdraft aloft of the shallow-mode disturbance in Case RIGID are somewhat weaker and stronger than those in Case SIMPLE, respectively. The difference is, however, negligibly small. Thus, whether or not the rigid lid exists at $z = 10.0$ km has virtually no effect on the

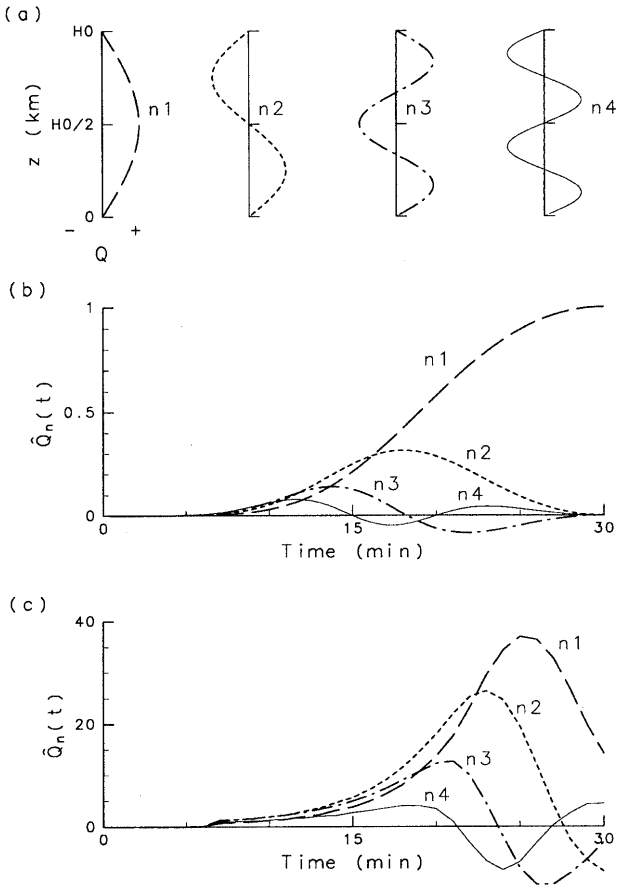

Fig. 8. (a) Vertical structure of the discrete vertical modes $\sin(n\pi z/H_0)$ for $n = 1$ ($n1$), $n = 2$ ($n2$), $n = 3$ ($n3$), and $n = 4$ ($n4$). Time variations of each vertical mode forcing $\hat{Q}_n(t)$ until 30 min for $n1$, $n2$, $n3$, and $n4$ modes of (b) the heating function $\hat{Q}(z,t)$ (Fig. 4b), and (c) the heating profiles within a convective cell for Case FULL (Fig. 4a).

gravity wave response until 30 min. Therefore, the results in Case SIMPLE can be plausibly interpreted using Eq. (4).

Figure 8b shows the time variation of each vertical-mode forcing $\hat{Q}_n(t)$. It is clear that the higher vertical-mode forcings have weaker amplitudes and higher frequencies. For example, the $n = 1$ mode ($n1$) forcing $\hat{Q}_1(t)$ reaches a maximum at 30 min, the $n = 2$ mode ($n2$) forcing $\hat{Q}_2(t)$ ceases at 30 min, with a maximum at 18 min, and the $n = 3$ mode ($n3$) forcing $\hat{Q}_3(t)$ is positive until 18 min and then turns negative until 30 min.

For simplicity, a case is considered where the x-dependence of the heating function is the Dirac delta function. Derived from the solution of Bretherton and Smolarkiewicz (1989), the linear response of the vertical velocity $w_n(x,t)$ to the heating $\hat{Q}_n(t)\delta(x)$, is proportional to the time-derivative of $\hat{Q}_n(t)$ as

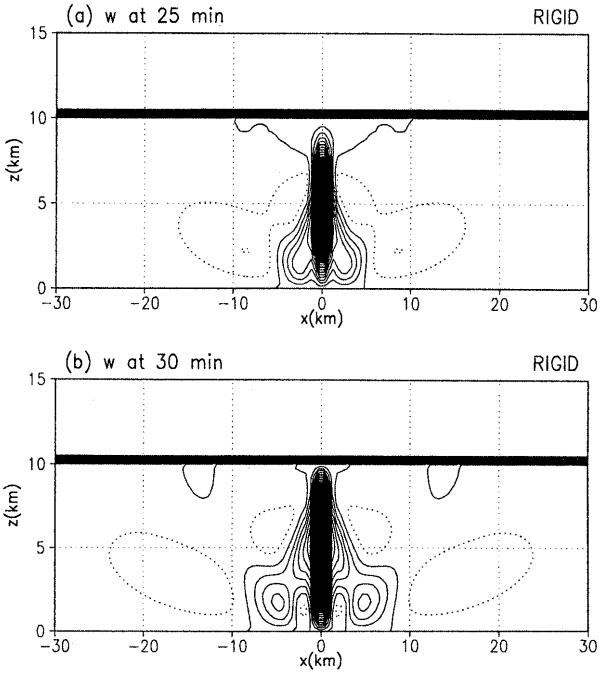

Fig. 9. As in Fig. 2, except for vertical velocity in Case RIGID. The contour interval is 0.01 m s^{-1}. The regions in which the vertical velocity exceeds 0.1 m s^{-1} are shaded. The thick horizontal line at $z =$ 10.0 km indicates the rigid upper boundary.

$$w_n(x,t) \propto -\frac{1}{c_n}\frac{d\hat{Q}_n(\tau)}{d\tau}\bigg|_{\tau=t-\frac{|x|}{c_n}}, \tag{5}$$

where $\delta(x)$ is the Dirac delta function, and c_n the speed of the wave given by

$$c_n = \frac{NH}{n\pi}. \tag{6}$$

Although Eq. (5) is derived from the infinitesimal-width case, the results from Case SIMPLE can be interpreted using Eq. (5). A similar approach has been applied to the interaction between gravity waves and tropical cloud clusters by Numaguti and Hayashi (2000).

For the $n1$ forcing, a response of downward motion would develop for $\tau(= t - |x|/c_n) < 30$ min, because $d\hat{Q}_1(\tau)/d\tau > 0$. For the $n2$ forcing, downward motion at low-levels would develop when $\tau < 18$ min, since $d\hat{Q}_2(\tau)/d\tau > 0$. Upward motion at low-levels, then, will develop for 18 min $< \tau <$ 30 min, because $d\hat{Q}_2(\tau)/d\tau < 0$. For the $n3$ forcing, downward motion at low-levels would develop when $\tau <$ 13 min, since $d\hat{Q}_3(\tau)/d\tau > 0$, and upward motion at low-levels, for 13 min $< \tau <$ 22 min, because $d\hat{Q}_3(\tau)/d\tau < 0$. Therefore, the shallow mode disturbance in Fig. 5 can be interpreted as the gravity wave response propagating after the decay of the $n2$ and $n3$ forcings if the heating function $Q(x,z,t)$

used in this study is considered as the sum of the $n1$, $n2$, and $n3$ forcings.

If the shallow mode disturbance is a response only to the $n2$ forcing, this disturbance would be symmetric in the z direction. The updraft at low levels of the shallow mode disturbance in Fig. 5, however, is stronger than the downdraft aloft, because this disturbance is a response not only to the $n2$ forcing, but also to the $n3$ forcing.

The time sequence of the heating profiles within the convective cell in Case FULL (Fig. 4a) were also decomposed into discrete vertical modes as $\sin(n\pi z/H_0)$. Note that a value of $H_0 = 8.8$ km is used in the decomposition of Case FULL, because the maximum height of the heating within the convective cell occurs at about 8.8 km. Figure 8c shows the time variation of each vertical mode in the Case FULL results. It should also be noted that the higher vertical-mode forcings have less amplitudes and higher frequencies as shown in Fig. 8c as well as was shown in Fig. 8b. Since the time variations of $\hat{Q}_1(t)$, $\hat{Q}_2(t)$, and $\hat{Q}_3(t)$ in Case FULL are similar to those in Case SIMPLE, the strong low-level updraft at 25 min in Case FULL (Fig. 2a) can be interpreted as the gravity wave response that has decoupled from the heated region, and propagates outward when the $n2$ and $n3$ forcings decrease, as was found in Case SIMPLE.

It should be noted that there are differences between the time variations of $\hat{Q}_2(t)$ and $\hat{Q}_3(t)$ in Case SIMPLE and Case FULL. The values of the prescribed heating $\hat{Q}_2(t)$ are always positive and $\hat{Q}_3(t)$ decreases to only a small negative value in Case SIMPLE (Fig. 8b). On the other hand, the heatings $\hat{Q}_2(t)$ and $\hat{Q}_3(t)$ in Case FULL decrease to large negative values (Fig. 8c). Attention is now returned to the time sequences of the heating profile in Case FULL and $Q(x,z,t)$ in Case SIMPLE (see Fig. 4). For Case FULL, a top-heavy heating profile occurred at 30 min, i.e., that the upper-tropospheric heating was stronger than the lower-tropospheric heating. On the other hand, the heating profile at 30 min in Case SIMPLE was vertically symmetrical with its maximum at $z = 5.0$ km. The differences between time variations of $\hat{Q}_2(t)$ and $\hat{Q}_3(t)$ in Case SIMPLE and Case FULL result from differences between the heating profiles at 30 min in Case SIMPLE and Case FULL.

Attention is now focused on why no strong low-level updrafts can be found in Case WIDE. The Fourier transform of the heating function $Q(x,z,t)$ for $0 < z < H_m(t)$ as given in Eq. (1) in the x direction results in

$$\tilde{Q} = Q_0 a e^{-ak} \frac{1-\cos(2\pi t/T)}{2} \sin\left(\frac{\pi z}{H_m(t)}\right), \quad (7)$$

where $\tilde{()}$ indicates the Fourier transform, and k is the horizontal wave number. The horizontal wavelength of the shallow-mode disturbance is about 10.0 km, while that of the deep-mode disturbance is about 30.0 km (Fig. 5b). Thus, from Eq. (7), the ratio of the heating amplitude of the shallow-mode to the deep-mode is $\exp(-2\pi a/10.0)/\exp(-2\pi a/30.0) = \exp(-2\pi a/15.0)$. The ratio is 8.1×10^{-1} for Case SIMPLE with $a = 0.5$ km, while 1.5×10^{-2} in Case WIDE with $a = 10.0$ km. These results indicate that not only the height increase (see Eq. (2)), but also the narrow width of $Q(x,z,t)$ are important for the shallow mode disturbance with a strong updraft at low levels. Therefore, the shallow-mode disturbance with a strong updraft at low levels is a particular response to a growing convective cell.

On the other hand, the ratio of the heating amplitude of the shallow-mode to the deep-mode is 6.6×10^{-1} when $a = 1.0$ km, corresponding to the horizontal width of 4.0 km. Thus, this ratio is not very sensitive to such a narrow-range change in the half-width a.

4.2 Vertical displacement

To calculate the time variation of vertical displacement resulting from the gravity wave response in Case FULL, a DRY experiment is performed, termed Case HEAT. The heating has the same vertical profile as was shown in Fig. 4a, but with 1/40 of the magnitude, and having a horizontal structure of $\cos(\pi x/2b)$ for $-b \le x \le b$ ($b = 1.0$ km). This experiment is carried out with the same initial sounding and vertical resolution as those in the MOIST experiments. The vertical displacement at $t = 33$ min for Case HEAT is shown in Fig. 10a. In Case FULL, new cells had formed at $x \approx \pm 2.0$ km at $t = 33$ min (Fig. 2b). The vertical displacement is calculated from the vertical velocity at each horizontal grid point and at $z = 1.5$ km, where the local maximum of latent heat first appeared at $x \approx \pm 2.0$ km in Case FULL. The region of upward displacement with the maximum at $x = 2.25$ km extends to $x = 3.5$ km, as shown in Fig. 10a. The region of upward displacement for Case HEAT nearly corresponds to the location where the new cell has formed in Case FULL (Fig. 2b). Therefore, the upward displacement resulting from the gravity wave response probably triggered the new cell found in Case FULL.

In order to examine the influence of the heating profile on the vertical displacement as a result of the gravity wave response, an additional DRY experiment is performed (Case SIMPLE2). Here the heating is the same in Case SIMPLE, but with a horizontal structure of $\cos(\pi x/2b)$ for $-b \le x \le b$ ($b = 1.0$ km). Figures 10b and c display the time variations of the vertical displacements calculated from the vertical velocity at $x = 2.0$ km and $z = 1.5$ km for Case HEAT and Case SIMPLE2, respectively. The vertical displacement found in Case

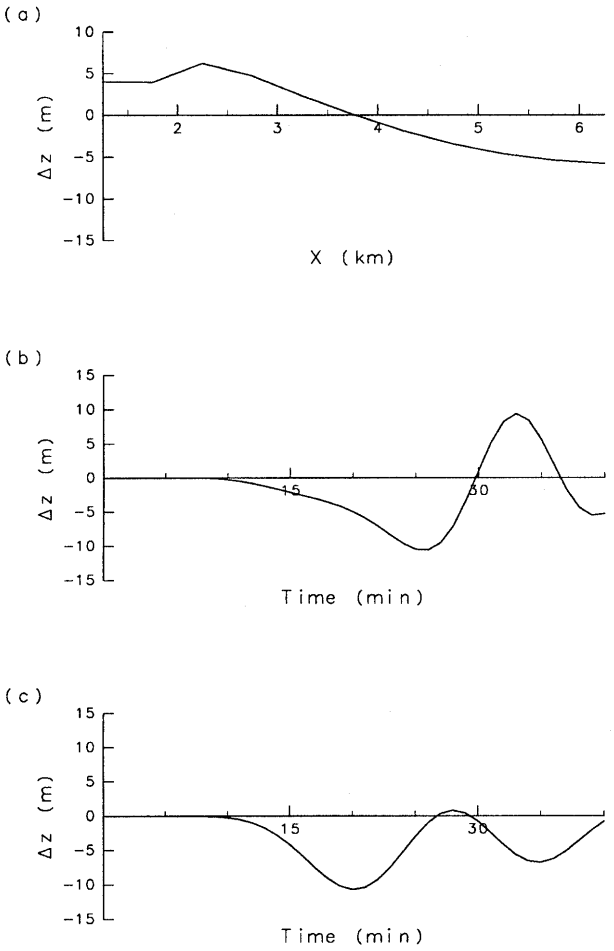

Fig. 10. (a) Vertical displacement at each horizontal grid and $z = 1.5$ km, outside the heated region at 33 min for Case HEAT. Time variations of the calculated vertical displacement at $x = 2.0$ km and $z = 1.5$ km, for (b) Case HEAT, and (c) Case SIMPLE2.

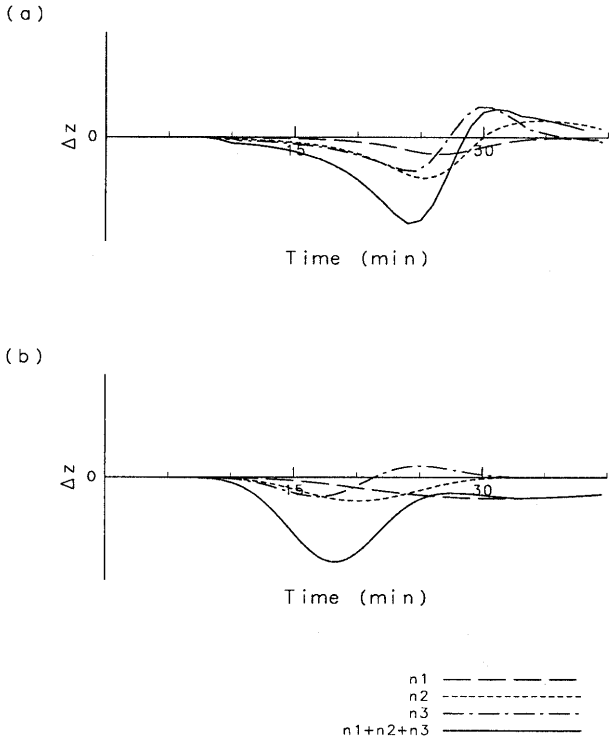

Fig. 11. Time variations of the estimated vertical displacement at $x = 2.0$ km and $z = 1.5$ km for (a) Case HEAT, and (b) Case SIMPLE2. The distributions are shown for the different mode forcings, according to the figure legend.

HEAT (Fig. 10b) is positive between 30–37 min, while that in Case SIMPLE2 (Fig. 10c) is negative, except for the small positive value at around 28 min. The next problem is to determine what causes the difference between the vertical displacements in Case HEAT and Case SIMPLE2.

From Eq. (5), the vertical displacement $\triangle z_n$ can be estimated from the response of vertical velocity $w_n(x,t)$ as

$$\triangle z_n \equiv \int_0^t w_n(x,t)dt \propto -\int_0^{t-\frac{|x|}{c_n}} \frac{1}{c_n}\frac{d\hat{Q}_n(\tau)}{d\tau}d\tau$$
$$= -\left[\frac{1}{c_n}\hat{Q}_n(\tau)\right]_0^{t-\frac{|x|}{c_n}}. \quad (8)$$

Figures 11a and b show time variations of the vertical displacement $\triangle z = \sum_{n=1}^{3} \triangle z_n$, at $x = 2.0$ km and $z = 1.5$ km from Case HEAT and Case SIMPLE2 as estimated by Eq. (8), respectively. The time variations of $\triangle z = \sum_{n=1}^{3} \triangle z_n$ in Figs. 11a and b roughly approximate those of the vertical displacements in Figs. 10b and c, respectively. Therefore, the vertical displacement due to the gravity wave response at $x = 2.0$ km and $z = 1.5$ km for a convective cell can be rather well estimated as $\triangle z = \sum_{n=1}^{3} \triangle z_n$ using Eq. (8).

For Case HEAT (Fig. 11a), $\triangle z_2$ and $\triangle z_3$ are positive between 30–40 min and 27–36 min, respectively, corresponding to the decrease in the $n2$ and $n3$ forcings to large negative values (see Fig. 8c). On the other hand, in Case SIMPLE2 (Fig. 11b), values of $\triangle z_2$ are always negative and those of $\triangle z_3$ reach a slightly positive value between 22–31 min. These results correspond to $\hat{Q}_2(t)$ being always positive and $\hat{Q}_3(t)$ decreasing to a small negative value (Fig. 8b). As a result, the vertical displacement $\triangle z$ in Case HEAT differs from that in Case SIMPLE2.

As was discussed in Section 4.1, the top-heavy heating profile at 30 min in Case FULL (Fig. 4a) forces $\hat{Q}_2(t)$ and $\hat{Q}_3(t)$ to decrease to large negative values (Fig. 8c). Therefore, the top-heavy heating profile at 30 min in Case FULL is very important for a net upward displacement.

Mapes (1993) also pointed out that a top-heavy heating profile was very important for "gregarious convection". The top-heavy heating profile in Mapes (1993) was due to the superimposition of the

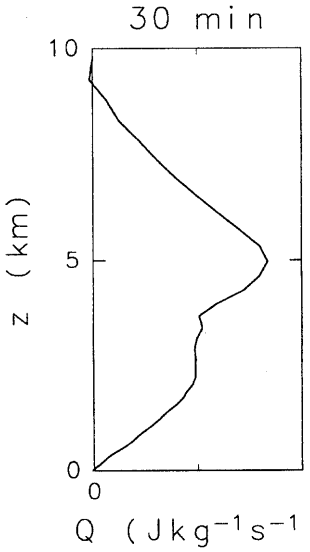

Fig. 12. The heating profile averaged from $x = -1.0$ km to $x = 1.0$ for Case NODRAG.

n = 1 mode, representing MCS convective precipitation, and the n = 2 mode, representing MCS stratiform precipitation. On the other hand, the heating profile in Fig. 4a does not include any heating that represents stratiform precipitation. Therefore, the top-heavy heating profile in the present study does not represent the precipitation type that Mapes (1993) studied.

Up to $t = 25$ min, the top-heavy heating profile does not appear seen in Fig. 4a. The difference between $t = 25$ and 30 min, is whether or not the downdraft at low-levels of the convective cell has formed. At 25 min, a downdraft is not formed at $x = 0.0$ km (Fig. 2a). By 30 min, a downdraft has formed below $z = 3.8$ km at $x = 0.0$ km (not shown, but clear in Fig. 2b). Therefore, it is concluded that the convective cell is cut off from the advection of water vapor by the downdraft at low-levels. Thus, condensational heating at low-levels in the convective cell decreases. This downdraft is mainly the result of the drag force associated with precipitation, because the top-heavy heating profile, the same as in Case FULL, is also found in Case NOEVAP (not shown) where the evaporation of rain is excluded. To confirm this conclusion, another MOIST experiment is performed (Case NODRAG) being the same as Case FULL except for the exclusion of the drag force due to rain. The heating profile at 30 min for Case NODRAG is shown in Fig. 12. The top-heavy heating profile, such as the profile found in Case FULL at $t = 30$ min (Fig. 4a), did not form, which confirms the above conclusion.

5. Summary and concluding remarks

In the present paper, the gravity wave response of a quiescent, two-dimensional, non-rotating atmosphere to a growing convective cell, using a non-hydrostatic compressible model, has been examined. A series of experiments were carried out, which were classified into two categories: (i) MOIST experiments that employed a parameterization of the Kessler warm cloud microphysics, and (ii) DRY experiments that were performed with a prescribed heating function.

The MOIST experiments revealed that a strong low-level updraft occurred near the convective cell during the later growing stage, even if evaporative cooling of rain was excluded. A new cell was then triggered in the region where the strong low-level updraft was found. In the DRY experiments, the heating function that roughly approximated two characteristics of the growing convective cell obtained in the MOIST experiment (Case FULL) was prescribed: 1) the height of the heating increased with time, and 2) the amplitude of the heating also increased with time. A DRY experiment (Case SIMPLE) with a half-width of $a = 0.5$ km also exhibited that the strong low-level updraft occurred during the later growing stage of the convective cell with the prescribed heating function.

A schematic diagram illustrating the gravity wave response to a growing convective cell up to the maximum stage is presented in Fig. 13. A shallow mode disturbance having a strong updraft at low levels occurs during the later growing stage of a convective cell (Fig. 13a). As a result of the increase in the height of heating (see the profile on the right of Fig. 13a), higher vertical mode forcings increase during the earlier growing stage of the convective cell, and decrease during the later growing stage. This disturbance can be interpreted as the gravity wave response to the higher vertical mode forcings.

For the shallow mode disturbance with a strong updraft at low levels, not only the increasing height of the heating, but also the narrow width of the heating are important. This indicates that the shallow mode disturbance with a strong updraft at low levels is a particular response to a growing convective cell.

The updraft at low levels of this disturbance results in a net vertical displacement, which probably triggers a new cell near the original cell. This results from the top-heavy heating profile (Fig. 13b) which forms at the maximum stage of development of the convective cell. The top-heavy heating profile is not due to the superimposition of the n = 1 mode representing MCS convective precipitation and the n = 2 mode representing MCS stratiform precipitation, as was suggested by Mapes (1993). It is concluded that the top-heavy heating profile is mainly due to the drag force associated with precipitation.

The shallow mode disturbance having a strong updraft at low levels is probably important for the structure and maintenance of meso-β-scale convec-

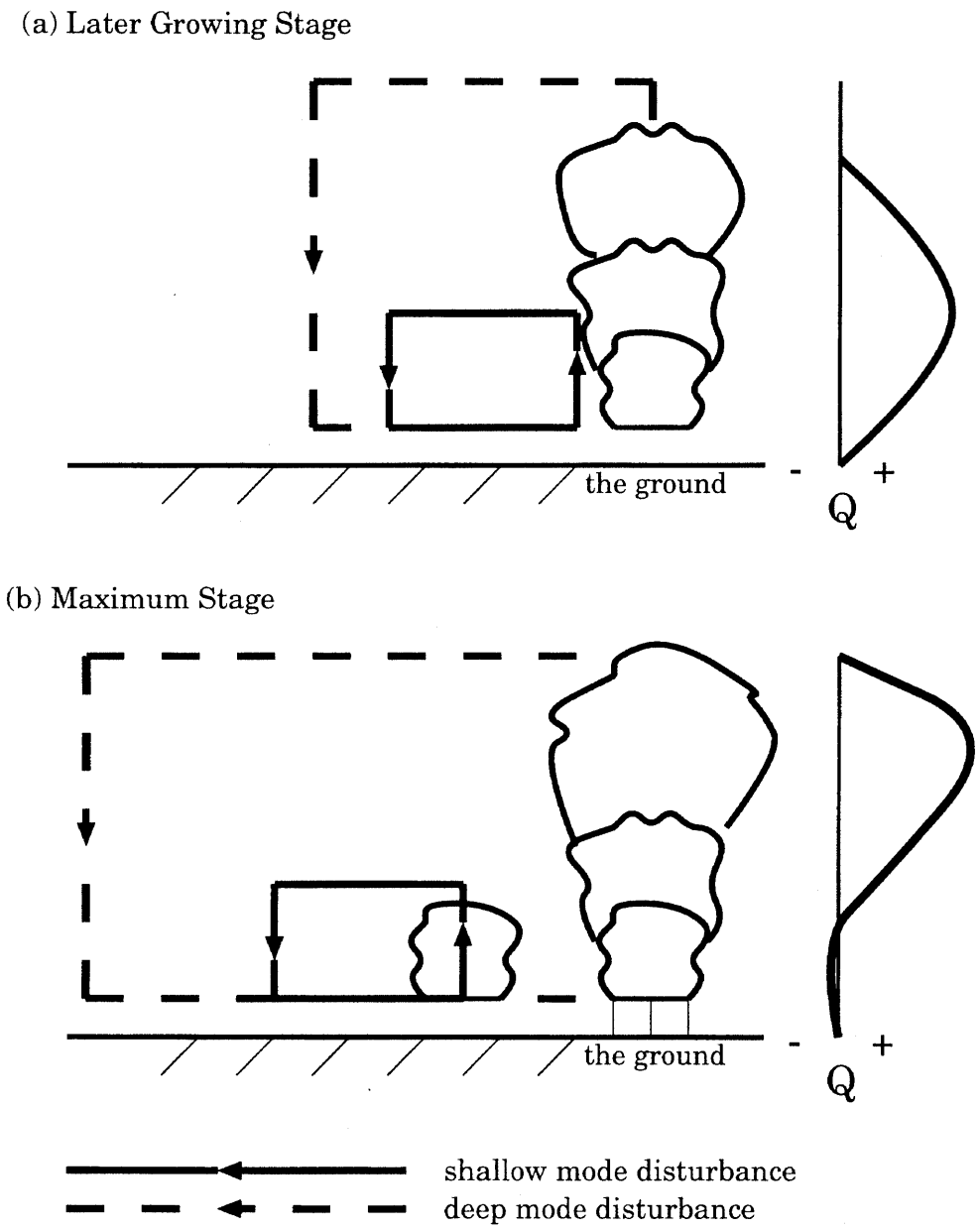

Fig. 13. A schematic diagram illustrating the gravity wave response to a convective cell until its maximum stage.

tive systems over tropical oceans. LeMone et al. (1998) reported that convective inhibition (CIN) is small (e.g., < 10 J kg^{-1} for COARE) over the tropical ocean, enabling convection to develop without an optimal state as described by Rotunno et al. (1998), but with only weak forcing. For example, slow-moving tropical cloud lines developed with weak low-level shear (see Fig. 8 of Barnes and Sieckman 1984), with the cold pool being shallow and weak (see Fig. 14 of LeMone et al. 1998).

The shallow mode disturbance with a strong updraft at low levels may play a certain role in the cell regeneration of a multicell squall line, where the interaction between the cold pool and the environmental vertical wind shear is important. The frequency of the generation of the shallow mode disturbance may determine the elapsed time between the development of successive convective cells within a multicell squall line. In the future, gravity waves in an environment with vertical wind shear will be investigated, using two- and three-dimensional numerical models.

Acknowledgments

Discussions with Dr. Toru Terao and Mr. Noriyuki Nishi, and comments by Dr. Shigeo Yoden were greatly appreciated. Thanks are extended to two anonymous reviewers for their comments on the

manuscript. The numerical experiments were conducted using the Advanced Regional Prediction System (ARPS) developed by the Center for Analysis and Prediction of Storms (CAPS), at the University of Oklahoma. CAPS is supported by the National Science Foundation and the Federal Aviation Administration, through a combined grant ATM92-20009. The computational time was provided by the KDK system at the Radio Atmospheric Science Center, Kyoto University. This work was partly supported by a research fellowship from the Japan Society for the Promotion of Science for Young Scientists (SS).

References

Barnes, G.M. and K. Sieckman, 1984: The environment of fast- and slow-moving tropical mesoscale convective cloud lines. *Mon. Wea. Rev.*, **112**, 1782–1794.

Bretherton, C.S. and P.K. Smolarkiewicz, 1989: Gravity waves, compensating subsidence, and detrainment around cumulus clouds. *J. Atmos. Sci.*, **46**, 740–759.

Durran, D.R. and J.B. Klemp, 1982: The effects of moisture on trapped mountain lee waves. *J. Atmos. Sci.*, **39**, 2490–2506.

Fovell, R.G. and Y. Ogura, 1988: Numerical simulation of a midlatitude squall line in two dimensions. *J. Atmos. Sci.*, **45**, 3846–3879.

——— and Y. Ogura, 1989: Effect of vertical wind shear on numerically simulated multicell storm structure. *J. Atmos. Sci.*, **46**, 3144–3176.

Klemp, J. and R. Wilhelmson, 1978: The simulation of three-dimensional convective storm dynamics.

LeMone, M.A., E.J. Zipser and S.B. Trier, 1998: The role of environmental shear and thermodynamics conditions in determinig the structure and evolution of mesoscale convective system during TOGA COARE. *J. Atmos. Sci.*, **55**, 3493–3518.

Mapes, B.E., 1993: Gregarious tropical convection. *J. Atmos. Sci.*, **50**, 2026–2037.

McAnelly, R.L., J.E. Nachamkin, W.R. Cotton and M.E. Nicholls, 1997: Upscale evolution of MCSs: Doppler radar analysis and analytical investigation. *Mon. Wea. Rev.*, **125**, 1083–1110.

Nicholls, M.E., R.A. Pielke and W.R. Cotton, 1991: Thermally forced gravity waves in an atmosphere at rest. *J. Atmos. Sci.*, **48**, 2561–2572.

Numaguti, A. and Y. Hayashi, 2000: Gravity-wave dynamics of the hierarchical structure of super cloud clusters. *J. Meteor. Soc. Japan*, **78**, 301–331.

Pandya, R.E. and M.J. Alexander, 1999: Linear stratospheric gavity wave above convective thermal forcing. *J. Atmos. Sci.*, **56**, 2434–2446.

——— and D.R. Durran, 1996: The influence of convectively generated thermal forcing on the mesoscale circulation around squall lines. *J. Atmos. Sci.*, **53**, 2924–2951.

———, ——— and C.S. Bretherton, 1993: Comments on "Thermally forced gravity waves in an atmosphere at rest". *J. Atmos. Sci.*, **50**, 4098–4101.

———, ——— and M.L. Weiseman, 2000: The influence of convective thermal forcing on the three-dimensional circulation around squall lines. *J. Atmos. Sci.*, **57**, 29–45.

Parsons, D., W. Dabberdt, H. Cole, T. Hock, C. Martin, A.L. Barrett, E. Miller, M. Spowart, M. Howard, W. Ecklund, D. Carter, K. Gage and J. Wilson, 1994: The Integrated Sounding System : Description and preliminary observations from TOGA COARE. *Bull. Amer. Meteor. Soc.*, **75**, 553–567.

Rotunno, R., J.B. Klemp and M.L. Weisman, 1988: A theory for strong, long-lived squall lines. *J. Atmos. Sci.*, **45**, 463–485.

Shige, S., 1999: Disturbances of 1–2 hour-periods observed in the tropical lower troposphere during the TOGA-COARE IOP. *J. Meteor. Soc. Japan*, **77**, 1123–1136.

Wakimoto, R.M., 1982: The life cycle of thunderstorm gust fronts as viewed Doppler radar and radiosonde data. *Mon. Wea. Rev.*, **110**, 1060–2082.

Webster, P.J. and R. Lukas, 1992: TOGA COARE: The coupled ocean-atmosphere response experiment. *Bull. Amer. Meteor. Soc.*, **73**, 1377–1416.

Xue, M., K.K. Droegemeier, V. Wong, A. Shapiro and K. Brewster, 1995: ARPS version 4.0 user's guide. CAPS, University of Oklahoma, 380pp. [Available from CAPS, University of Oklahoma, Norman, OK 73019.]

積雲対流の周囲に励起される重力波

重　尚一・里村雄彦
(京都大学大学院理学研究科)

圧縮性方程式系を解く非静水圧モデルを用い、成長する対流セルに対する静止大気の重力波応答について調べた。(1) Kessler の雲物理過程を導入した“湿潤”実験と (2) 雲物理過程の代わりに加熱関数を導入した“乾燥”実験の 2 つに分類される一連の実験を行った。乾燥実験で用いられた加熱関数は、湿潤実験における対流セルの加熱に基づいて与えられている。

下層に強い上昇流を持った浅い鉛直モードの擾乱が、成長段階後期の対流セル近くで励起されていることが示された。この浅い鉛直モードの擾乱は、対流セルの成長段階初期に増加し成長段階後期に減少する鉛直高波数の加熱強制に対する重力波応答と解釈できる。その励起には、加熱が鉛直方向に成長することと加熱の水平方向の幅の狭さが重要であり、成長する対流セルに特有な応答であることがわかる。

浅い鉛直モードの擾乱の下層の上昇流は、正味で正の鉛直変位をもたらす。これは、対流セルが最大高度に成長した時に加熱が上層で大きくなるためである。古い対流近くでの新たな対流セルの誘起は、この正の鉛直変位によると考えられる。